



**HAL**  
open science

## On the determination of acoustic emission wave propagation velocity in composite sandwich structures

Yuan Wu, Marianne Perrin, Marie-Laetitia Pastor, Pascal Casari, Xiaojing Gong

► **To cite this version:**

Yuan Wu, Marianne Perrin, Marie-Laetitia Pastor, Pascal Casari, Xiaojing Gong. On the determination of acoustic emission wave propagation velocity in composite sandwich structures. *Composite Structures*, 2020, 259, pp.113231. 10.1016/j.compstruct.2020.113231 . hal-03003145

**HAL Id: hal-03003145**

**<https://hal.science/hal-03003145>**

Submitted on 3 Feb 2023

**HAL** is a multi-disciplinary open access archive for the deposit and dissemination of scientific research documents, whether they are published or not. The documents may come from teaching and research institutions in France or abroad, or from public or private research centers.

L'archive ouverte pluridisciplinaire **HAL**, est destinée au dépôt et à la diffusion de documents scientifiques de niveau recherche, publiés ou non, émanant des établissements d'enseignement et de recherche français ou étrangers, des laboratoires publics ou privés.



Distributed under a Creative Commons Attribution - NonCommercial 4.0 International License

# ON THE DETERMINATION OF ACOUSTIC EMISSION WAVE PROPAGATION VELOCITY IN COMPOSITE SANDWICH STRUCTURES

Yuan Wu<sup>a</sup>, Marianne Perrin<sup>\*a</sup>, Marie-Laetitia Pastor<sup>a</sup>, Pascal Casari<sup>b</sup> and Xiaojing Gong<sup>a</sup>

<sup>a</sup>*Institut Clément Ader (ICA), CNRS, UMR 5312, University of Toulouse, UPS, 1 rue Lautréamont, 65000 Tarbes, France.*

<sup>b</sup>*Institut de Recherche en Génie Civil et Mécanique, GeM-E3M, CNRS, UMR 6183, University of Nantes, Saint Nazaire, France.*

\* Corresponding author.

E-mail address: marianne.perrin@iut-tarbes.fr ([Marianne Perrin](mailto:marianne.perrin@iut-tarbes.fr)).

## ABSTRACT

This work focuses on the rapid determination of Acoustic Emission (AE) wave propagation velocity in composite laminate and sandwich structures using a closed-form formula. Firstly, a classical closed-form model proposed in the literature is extended to determine the acoustic wave velocity in any direction in a composite laminate or sandwich structure; then a corrective factor has been defined to improve the calculation accuracy; finally, a parameter, called correlation ratio has been introduced to describe the relation between acoustic wave velocity in the composite skin and that in the sandwich panel. This strategy has been validated by two types of composite sandwich panels: one is honeycomb sandwich structures with CFRP composite laminate skins; the other is balsa sandwich with GFRP skins. It is demonstrated that acoustic wave velocity in the sandwich is dominated by the skin property, namely the elastic modulus of the skin, the density of the constituents, the core and skin thickness. Moreover, only by measuring the velocity in one direction, the velocity in any direction of composite structures can be predicted accurately and quickly. This work lays the first foundations for the establishment of numerical and experimental models necessary to improve the damage localization of composite structures.

## Keywords:

Acoustic Emission (AE); Composite sandwiches; Composite laminates; Acoustic wave velocity.

## 1. Introduction

Thanks to the outstanding mechanical behaviors such as high specific stiffness and strength, good bending resistance and energy absorption property, honeycomb sandwich structures with Carbon Fiber Reinforced Polymer (CFRP) skins have become widely applied in the aeronautic industry, while the balsa sandwich with Glass Fiber Reinforced Polymer (GFRP) skins is more popular in the naval field due to lower costs [1-3]. However, the typical anisotropic properties of honeycomb and balsa materials make it difficult to characterize the complicated mechanical behavior of the whole sandwich structure [4]. Specifically, due to the unique cell shape of the honeycomb structure, the shear stiffness in the L orientation is usually higher than that in the W direction (see Fig. 1) [5]. Balsa wood is less stiff and weaker in the tangential and radial directions, compared to the axial direction. It has been proved that the mechanical properties of balsa material in the three directions are as a function of the density [6-8]. Concerning composite laminate skins, their stiffness and strength also greatly depend on the material constituents: fiber and matrix, stacking sequence and the thickness. Therefore, the nature of laminate skins, thickness and density of the core material determine together the stiffness and the strength of the composite sandwich structure [9]. Thus, it is of great challenge to quantify the stiffness degradation caused by damage evolution in the complex sandwich structure under loading. It still remains a hotspot to locate the damage zone and identify the damage type such as skin delamination, fiber breakage, skin-core debonding and core shear damage [10-11]. Over the last decades, Non Destructive Testing (NDT) methods have become effective tools to detect and monitor the damage evolution in composite structures, especially Acoustic Emission (AE) and ultrasonic method [12-13].

AE technique listens to the radiation and propagation of elastic waves in a structure when there are growing and irreversible internal changes. As a promising Structural Health Monitoring (SHM) method developed in recent years, AE technique has increasingly played an important role in the damage mechanism identification and classification, damage source localization and severity assessment, owing to its dynamic and continuous monitoring of the damage initiation and evolution in real time [14-16]. Particularly, the most important concerns are to know exactly when and where damages appear, making it necessary to precisely characterize the acoustic wave propagation property, including wave attenuation and velocity [17-18]. In order to measure the acoustic wave propagation velocity, ultrasonic method which is based on the acoustic wave reflection through the thickness is usually used for composite laminates. Indeed, it needs a probe for the signal emission and reception, and the wave mainly propagates along the depth. As a result, the measured velocity is limited by the local region, making it more inaccurate for the anisotropic structures, especially when internal damages exist [19-20]. In contrast, without the repeated scanning procedure, AE method is more efficient by simply generating the pencil lead breaks (Hsu-Nielsen test) [21-22] on the structure surface to simulate the artificial acoustic wave source and using fixed sensors to receive the acoustic signals in any direction and position.

Theoretically, for infinite thin plates, when the wavelength is much larger than the plate thickness, Lamb wave is thought to be the dominated propagation wave. The understanding of the acoustic wave modes is usually based on the classical plate wave theory, which assumes that there exist two wave modes, the extensional/longitudinal ( $S_0$ ) wave and flexural wave ( $A_0$ ). Due to the Poisson effect, both modes consist of the in-plane and out-of-plane components. But the traditional extensional wave velocity equation is used to predict only the in-plane wave propagation, while the flexural wave velocity equation mainly presents the out-of-plane mode [23]. In application, wideband sensors [24] are often located on the surface of the plate to distinguish between the two wave modes, where the extensional wave having higher velocity and frequency. H. Khon [25] found that the delay time of the flexural mode will decrease when increasing the frequency and reducing the sensor-source distance. Michael R. Gorman [26] investigated the effects of the artificial AE source orientation angle on the velocity, showing that the extensional wave is the predominant at the smaller pencil lead breaking angle. Consequently, using the narrowband sensor with relatively lower resonance frequency and the larger sensor-source distance can reduce the interference of the slower flexural mode on the received extensional wave signals.

Nowadays, most researches concerning the application of AE technique in composite structures are concentrated on thin laminates [27]. Few works on the AE wave propagation property [28-30] could be found about composite sandwich structures, especially on the theoretical AE wave velocity analysis. For an isotropic plate or thin orthotropic laminate, AE wave velocity is considered as a function of in-plane Young's modulus, Poisson's ratio, and the density of the material [21-23]. However, it is not clear whether the traditional acoustic wave velocity formula can be applicable to thick anisotropic and heterogeneous sandwich structures. In order to apply AE technique to monitor complex damage evolution in composite sandwich structures, the further investigation and demonstration on the AE wave velocity shall be necessary and worthy. These elements will be the new construction basis of numerical and experimental models necessary for the improvement of the damage localization and the implementation of repair operations. Since the degradation of materials is directly related to the variation of propagation properties of acoustic waves, it will be necessary to include corrective terms being able to integrate internal changes of the monitored structure in real time in

the models. Finally, the real-time communication between tests and calculations will be an essential step to be considered in the evolution of models.

Therefore, the work presented here consists in understanding which parameters influence the velocity in composite sandwich structures. Firstly, AE wave velocities of two kinds of composite laminates were measured and compared with those from a theoretical model. And then a corrective factor has been introduced to improve the prediction of AE wave velocity by the closed-form theoretical model for any composite laminate. Finally, to describe the relation between AE wave velocity in the composite laminate skin and that in the sandwich panel, a correlation ratio has been firstly proposed.

## 2. Materials and testing methods

### 2.1. Materials and specimens

Two different sandwiches (see Fig. 2) and the corresponding constituent panels are tested in this work. All sandwich panels have two identical symmetrical skins. For the CFRP-honeycomb sandwich, tests on constituents have been performed on single CFRP laminates made from three plies of unidirectional prepreg with lay-up of  $[0^\circ/90^\circ/0^\circ]$ , CFRP-honeycomb sandwich panels using CFRP  $[0^\circ/90^\circ/0^\circ]$  skins and single core with different materials and thicknesses. The CFRP-honeycomb sandwich specimen's dimensions and material constants [31] are shown in Table 1 and Table 2 where  $E_1$  is longitudinal modulus,  $E_2$  is transverse modulus,  $G_{12}$  is in-plane shear modulus,  $\nu_{21}$  is Poisson's ratio of unidirectional laminate and  $\rho$  is the material density. For the GFRP-balsa sandwich, tests have been performed on the 3-layer woven balanced GFRP laminate of  $[0^\circ]_3$ , a single balsa wood panel and the GFRP-balsa sandwich panel with balsa core and  $[0^\circ]_3$  GFRP skins. The GFRP-balsa sandwich specimen's dimensions and material constants [32-33] are shown in Table 3 and Table 4. In Fig. 2. (b), we can notice the particular structure of the balsa, which consists of small pieces glued to each other, and thus a large plate is formed.

### 2.2. Testing methods

The typical AE system mainly includes the pencil, the sensors, the couplant, the pre-amplifier, the analogue filters and the acquisition system (Mistras AEwin software with USB-AE node). Among them, the selection of the proper sensor, threshold, pre-amplifier, analog-filter, Peak Definition Time (PDT), Hit Definition Time (HDT) and Hit Lockout Time (HLT) are the most important factors affecting the testing sensitivity and accuracy. First of all, concerning the choice of sensor, due to the difference of the attenuation property of sandwich constituent material, a compromise has been made by using R6 $\alpha$  sensor whose resonance frequency is 60 kHz for all the specimens [34]. The threshold determines the system sensitivity to the environmental noise, which is set by 30 dB. The pre-amplifier is 40 dB, and the analog-filter is in the range of 20 kHz -1 MHz. PDT is 35  $\mu$ s, HDT is 150  $\mu$ s, and HLT is 300  $\mu$ s. All these parameters were validated during the preliminary tests.

For each panel mentioned above, according to Hsu-Nielsen test, pencil lead breaking is conducted at least 10 times for AE wave propagation in one direction, and the test is repeated every 15° between 0° and 90° to study the direction effects on AE wave velocity (see Fig. 3). The velocity has been measured on the basis of the difference of the arrival times between the two sensors mounted on top surface of the panel (see Fig. 4), as given by Eq. 1:

$$v = \frac{D}{\Delta t} = \frac{D}{t_2 - t_1} \quad (1)$$

Where,  $t_2$  and  $t_1$  are the arrival times at the maximum amplitude at each sensor, respectively;  $D$  is the distance between the two sensors  $S_1$  and  $S_2$ , which is 100 mm;  $D_1$  is the distance between  $S_1$  and the source, which is 50 mm.

As mentioned in the introduction, the plate wave theory [21-23] is often used to analyze the acoustic wave propagation velocity when the thickness is much smaller than the other two dimensions of the plate. It is complicated to distinguish between the extensional and flexural wave modes, but the velocity measured in the standard Hsu-Nielsen test is proved to be dominated by the extensional wave [22, 26]. For an infinite isotropic plate, the longitudinal wave velocity,  $C_L$  can be expressed as Eq. 2:

$$C_L = \sqrt{\frac{E}{\rho(1-\nu^2)}} \quad (2)$$

Where  $\rho$  is the specimen density,  $E$  is Young's modulus,  $\nu$  is Poisson's ratio.

For an orthotropic composite laminated plate,  $C_L$  is thought to be related to the in-plane longitudinal elastic modulus,  $E_{11}$ . The formula is often given by Eq. 3 [23]:

$$C_L = \sqrt{\frac{E_{11}}{\rho(1-\nu_{21}^2)}} \quad (3)$$

Where  $E_{11}$  and  $\nu_{21}$  denote the in-plane Young's modulus and Poisson's ratio respectively in 1 direction.

In this work, in order to determine the extensional wave velocity in any direction,  $x$  is defined by an angle  $\theta$  measured from 1 direction, we try to extend Eq. 3 to Eq. 4 as following:

$$C_L(\theta) = \sqrt{\frac{E_x(\theta)}{\rho (1-\nu_{yx}(\theta)^2)}} \quad (4)$$

Where  $\rho$  is the structure density;  $E_x(\theta)$  and  $\nu_{yx}(\theta)$  are Young's modulus and Poisson's ratio in the measured direction  $x$ , associated with angle  $\theta$ ; recall that  $\nu_{yx}(\theta)$  denotes the ratio of strain in the  $y$  direction over that in the  $x$  direction when there is stress in the  $x$  direction. Herein the composite constants  $E_x(\theta)$  and  $\nu_{yx}(\theta)$  in any direction  $\square$  can be determined easily by the classical laminate theory.

### 3.Results and discussions for composite laminates

#### 3.1. AE wave velocity in the CFRP laminate skin

AE wave velocity in the thin CFRP skin of  $[0^\circ/90^\circ/0^\circ]$  is tested between  $0^\circ$  and  $90^\circ$  with a measurement step at  $15^\circ$ , and it is compared to the calculated velocity by Eq. 4, as shown in Fig. 5. The measured velocities (red line) and analytical values (purple dotted line) show the similar variation tendency along different directions, with the highest velocity in  $0^\circ$  and the lowest in  $60^\circ$ . The maximum error between the measurements and calculated velocities by Eq. 4 is 15.57% in  $15^\circ$ , and the minimum error is 12.92% in  $0^\circ$ .

It is obvious that the direction has large influence on the AE wave velocity, with the max difference of 3400 m/s between  $0^\circ$  and  $60^\circ$ . The velocity in  $0^\circ$  with two plies of fibers is a little higher than that in  $90^\circ$  direction with only one ply of fibers. In conclusion, the farther it is away from the most fiber orientation, the lower the velocity will be. It indicates that the effects of the propagation direction on the velocity shall be considered when locating the damages in the composite structures.

According to the consistent variation tendency, it gives us an inspiration that only by measuring the AE wave velocity in the  $0^\circ$  direction where the error is the smallest, we can modify Eq. 4 to get the more precise velocity in any direction just by introducing a corrective factor,  $a$ . If this corrective factor is defined as the ratio of measured  $C_L$  in  $0^\circ$  over the  $C_L$  calculated by Eq. 4 in the same direction, the velocity in any direction can be determined by Eq. 5:

$$C_L(\theta) = a \cdot \sqrt{\frac{E_x(\theta)}{\rho (1-\nu_{yx}(\theta)^2)}} \quad (5)$$

$$\text{Where } a = \frac{C_L^{\text{Measured}}(\theta=0^\circ)}{C_L^{\text{Calculated}}(\theta=0^\circ)} = \frac{C_L^{\text{Measured}}(\theta=0^\circ)}{\sqrt{E_x(\theta=0^\circ)/\rho (1-\nu_{yx}(\theta=0^\circ)^2)}}$$

Applying this idea to the case of the thin CFRP skin, the corrective factor can be determined:

$$a = \frac{C_L^{\text{Measured}}(\theta=0^\circ)}{C_L^{\text{Calculated}}(\theta=0^\circ)} = \frac{8796 \text{ m/s}}{7660 \text{ m/s}} = 1.148$$

The results obtained from measurements, Eq. 4 and Eq. 5 are compared in Fig. 5. It can be seen that the max error between the measured velocity (red line) and the calculated value (blue dotted line) by Eq. 5 is only 3.05% in  $15^\circ$ , which is largely reduced, compared to that of 15.57% in  $15^\circ$  if using Eq. 4.

In fact, the corrective factor,  $a$ , reflects the system error between the theoretical acoustic wave formula and the real propagated velocity in the composite structure, such as the influence of other wave propagation modes, the sensors' distance and sensitivity, as well as the test environment like sound noises. This factor is considered constant for a given composite system, independent of the AE wave propagation direction.

#### 3.2. AE wave velocity in the GFRP laminate skin

Similarly, AE wave velocity in the 3-layer woven GFRP skin panels is tested every  $15^\circ$  between  $0^\circ$  and  $90^\circ$ , as shown in Fig. 6. In this case, by application of Eq. 5, the corrective factor is obtained by:

$$a = \frac{C_L^{\text{Measured}}(\theta=0^\circ)}{C_L^{\text{Calculated}}(\theta=0^\circ)} = \frac{3967 \text{ m/s}}{3212 \text{ m/s}} = 1.212$$

The comparison of the measured velocities (red line) and calculated values by Eq. 4 (purple dotted line) and Eq. 5 (blue dotted line) are plotted in Fig. 6. The measured and analytical velocities show the similar variation tendency along different directions, with the highest in  $90^\circ$  and the lowest in  $45^\circ$ . Compared to the max difference of 3400 m/s in the CFRP panel, the propagation direction has smaller effects on the velocity variation in the woven GFRP panel, with the max measured difference of only 540 m/s between  $0^\circ$  and  $45^\circ$ . It demonstrates further that the  $[0^\circ/90^\circ/0^\circ]$  CFRP and the 3-layer woven GFRP laminates have the different behavior, which is mainly because the former has the most fiber oriented at  $0^\circ$ , while the later has the same number of fibers oriented at  $0^\circ$  and  $90^\circ$ .

The max error between the test and calculation results by Eq. 4 is 22.65% in  $60^\circ$ , and the minimum error is 17.51% in  $0^\circ$ . By using the modified formula Eq. 5, the max error is highly reduced, with only 6.23% in  $60^\circ$ .

## 4. Results and discussions for composite sandwich structures

### 4.1. AE wave velocity in CFRP-honeycomb sandwich structures

#### 4.1.1. Comparison of the measured velocity and calculated value

Similar to the approach applied to the pure laminate skin, AE wave velocity between  $0^\circ$  and  $90^\circ$  in the CFRP-honeycomb sandwich specimen A is firstly tested, and compared to the analytical results from Eq. 4 (purple dotted line) and the modified model Eq. 5 (blue dotted line), as plotted in Fig. 7, where the corrective factor is determined by:

$$a = \frac{C_L^{Measured}(\theta=0^\circ)}{C_L^{Calculated}(\theta=0^\circ)} = \frac{7716 \text{ m/s}}{6723 \text{ m/s}} = 1.148$$

It is observed that the test and theoretical velocities show a similar variation tendency along different directions, with the highest velocity in  $0^\circ$  and the lowest in  $60^\circ$ . The max error between test and calculation results by the modified Eq. 5 is largely reduced to only 3.69% in  $30^\circ$ , compared to the max 13.04% by Eq. 4. It is verified that the improved AE wave velocity formula Eq. 5 can also be effective for the thick composite sandwich structure. In this way, plenty of time and experimental efforts can be saved.

#### 4.1.2. Correlation between AE wave velocity in the skin and sandwich

Fig. 8 compares the measured AE wave velocities in sandwich A and those measured on the pure laminate skin of CFRP [ $0^\circ/90^\circ/0^\circ$ ]. It can be seen that the velocity in the skin is always higher than that in the sandwich whatever the acoustic wave propagation direction; their variation along different directions has the similar tendency with the highest velocity in  $0^\circ$  and lowest in  $60^\circ$ .

A possible explanation for this phenomenon is that the AE wave velocity in a sandwich structure is dominated by the skin property, and the existence of honeycomb core with much lower modulus and density mainly contributes to the small velocity decrease. Moreover, considering the effects of coupling of multiple propagation wave modes, the out-of-plane flexural mode contributes more to the acoustic wave attenuation in thicker sandwich structure, which results in the higher velocity dispersion compared to the thinner laminate skin. In addition, the air in the hollow honeycomb core cell may cause the acoustic wave attenuation.

The similar velocity variation tendency indicates that the direction effects on the elastic modulus and Poisson's ratio result in the variation of AE wave velocity along different directions in both the laminate and sandwich structures. From this observation, it is now interesting to know whether there is a simple relationship between the wave propagation velocity of a composite sandwich structure and that of their composite skin.

Based on multimaterial beam theory [35], the equivalent modulus of sandwich structure  $E_s(\theta)$  can be obtained by the combination of that of the core and that of the two skins:

$$E_s(\theta) \cdot A = E_f(\theta) \cdot \frac{2h_f}{h_s} \cdot A + E_c(\theta) \cdot \frac{h_c}{h_s} \cdot A$$

Where  $A$  is the cross-section area of a sandwich beam;  $E_f(\theta)$  and  $E_c(\theta)$  are the elastic modulus of the skin and the core, respectively.  $h_s$ ,  $h_c$  and  $h_f$  are the thickness of the sandwich, of the core and of the skin, respectively.

Then  $E_s(\theta)$  can be expressed as:

$$E_s(\theta) = E_f(\theta) \cdot \frac{2h_f}{h_s} + E_c(\theta) \cdot \frac{h_c}{h_s} \quad (6)$$

Using the specimen dimensions and material parameters in Table 1 and Table 2, the density of sandwich A can be obtained by Eq. 7:

$$\rho_s = \frac{2\rho_f \cdot h_f + \rho_c \cdot h_c}{h_s} \quad (7)$$

Hence,  $\rho_s(A) = 183 \text{ kg/m}^3$ .

Substituting Eq. 6 and Eq. 7 into Eq. 4, AE wave velocity in a sandwich structure can be given by Eq. 8:

$$C_{Ls}(\theta) = \sqrt{\frac{E_s(\theta)}{\rho_s(1-\nu_{yx}(\theta)^2)}} = \sqrt{\frac{2E_f(\theta) \cdot h_f + E_c(\theta) \cdot h_c}{2\rho_f \cdot h_f + \rho_c \cdot h_c} \cdot \frac{1}{(1-\nu_{yx}(\theta)^2)}} \quad (8)$$

Eq. 8 indicates that the acoustic wave velocity in the sandwich structure is mainly determined by the elastic modulus, the density and thickness of the constituent materials. For sandwich structure,  $E_c$  is much smaller than  $E_f$  (see Table 2 and 4). In the case of  $E_c(\theta)h_c/2E_f(\theta)h_f < 5\%$ , the contribution of  $E_c(\theta)$  to  $E_s(\theta)$  can be ignored with less than 5% error, which means  $h_c < 0.1h_f E_f(\theta)/E_c(\theta)$ , and then Eq. 6 becomes:

$$E_s(\theta) = E_f(\theta) \cdot \frac{2h_f}{h_s} = E_f(\theta) \cdot \frac{2h_f}{2h_f + h_c} = E_f(\theta) \cdot \frac{2}{2 + \frac{h_c}{h_f}} \quad (9)$$

This expression shows that the modulus of sandwich can be obtained from that of the skin multiplied by a geometrical coefficient:  $2/(2+h_c/h_f)$ . The higher the ratio of the core thickness over that of the skin is, the lower the

contribution of the skin modulus will be. If the skin thickness remains the same, the thicker core will result in lower elastic modulus of sandwich structure.

According to the theoretical calculation, Poisson's ratios of the skin and the sandwich are nearly the same in the same direction for commonly used sandwiches. Hence, from the AE wave velocity formula, the correlation ratio of the wave velocity in the sandwich over that in the skin,  $R$ , is proposed by Eq. 10:

$$R = \frac{c_{Ls}(\theta)}{c_{Lf}(\theta)} = \sqrt{\frac{E_s(\theta)}{E_f(\theta)} \cdot \frac{\rho_f}{\rho_s}} \quad (10)$$

Substituting Eq. 7 and Eq. 9 into Eq. 10, it becomes:

$$R = \frac{c_{Ls}(\theta)}{c_{Lf}(\theta)} = \sqrt{\frac{2h_f}{2h_f+h_c} \cdot \frac{\rho_f \cdot (2h_f+h_c)}{2\rho_f \cdot h_f + \rho_c \cdot h_c}} = \sqrt{\frac{2\rho_f \cdot h_f}{2\rho_f \cdot h_f + \rho_c \cdot h_c}} = \sqrt{\frac{2}{2 + \frac{\rho_c h_c}{\rho_f h_f}}} \quad (11)$$

Eq. 11 works well with a condition of  $h_{c-\max} < 0.1h_f E_f(\theta)/E_c(\theta)$ . It signifies that the correlation between AE wave velocity in the sandwich and in their skin is mainly determined by the density and thickness of the constituent materials.

Theoretically, when  $h_c$  is 0,  $R$  becomes 1, corresponding to the pure laminate skin. If  $h_c \neq 0$ ,  $0 < R < 1$ . Considering the application condition of Eq. 11,  $h_c$  has a max limitation by  $h_{c-\max} < 0.1h_f E_f(\theta)/E_c(\theta)$ . The main problem is that the different variation tendency of elastic modulus of the core and skin along different directions makes it complex to give an accurate value of  $E_f(\theta)/E_c(\theta)$ . Furthermore, the system error of the use of  $R$  could be caused by the same reasons as those for Eq. 5. To simplify the analysis, we predict  $h_{c-\max}$  by modulus of core and skin in  $0^\circ$  direction. Although it may cause larger error between  $15^\circ$  and  $75^\circ$  directions, the average error is proved to be acceptable.

For CFRP-honeycomb (Nomex) sandwiches (A and C), the  $h_{c-\max}$  at  $\theta = 0^\circ$  for Eq. 11 is about 60 mm from the material parameters in Table 1 and Table 2. Applying Eq. 11 to sandwich A ( $h_c=18\text{mm}$ ),  $R$  equals to 0.87. This value is compared to the measured results in Fig. 9. Good agreement has been observed. The average measured ratio  $R$  in different directions is about 0.86. It demonstrates that Eq. 11 can be used to predict the AE wave velocity in a sandwich structure from the corresponding velocity in the skin. Thus, there is no need to make lots of efforts to repeat Hsu-Nielsen tests to study AE propagation properties of both the skin and sandwich structure in all the directions. In fact, it can save at least 4 hours of test time to obtain the precise velocities in both the skin and sandwich in all directions.

#### 4.1.3. Validation of the proposed model using correlation ratio $R$

In order to validate the above proposed approach, the CFRP-honeycomb sandwich specimen B (aluminum core with  $h_c=30$  mm) and C (Nomex core with  $h_c=60$  mm) have been studied. The AE wave velocities between  $0^\circ$  and  $90^\circ$  in sandwich B and C were measured and compared with those of sandwich A (Nomex core with  $h_c=18$  mm) and those of the skin in Fig. 10. The measured velocities in the skin, sandwich A, B and C show the similar variation tendency along different directions, with the highest velocity in  $0^\circ$  and the lowest in  $60^\circ$ . The thicker the core is, the lower the wave velocity in sandwich structure will be. The farther it is away from the most fiber direction, the larger the velocity difference between the different sandwich panels will be. It means that the core thickness has larger effects on the acoustic wave velocity in the directions with fewer fiber contents.

The  $h_{c-\max}$  at  $\theta = 0^\circ$  is about 60 mm for CFRP-honeycomb (Nomex) sandwiches (A and C) and 200 mm for CFRP-honeycomb (Aluminum) sandwich (B). Now if Eq. 11 is applied to sandwich B and C, the correlation ratio  $R$  of sandwich B and C can be obtained, equals to 0.82 and 0.70, respectively. Fig. 11 compares the theoretical and measured correlation ratio of sandwich B and C. The average tested correlation ratio of sandwich B is 0.84, and it is 0.80 for sandwich C. Obviously, the thicker the core is, the larger the error between the tested ratio and theoretical value by Eq. 11 will be. One explanation could be that the contribution of the Poisson's ratio of the core should not be ignored when the core thickness is much larger. Then going back to Eq. 8, the correlation ratio becomes:

$$R = \frac{c_{Ls}(\theta)}{c_{Lf}(\theta)} = \sqrt{\frac{2}{2 + \frac{\rho_c h_c}{\rho_f h_f}} \cdot \frac{(1-\nu_f(\theta)^2)}{(1-\nu_s(\theta)^2)}} \quad (12)$$

Eq. 12 shows that the correlation ratio can be affected by the direction via Poisson's ratio, which can be reflected by the red curves in Fig. 9 and Fig. 11. An interesting phenomenon is that correlation ratio by Eq. 12 shows the similar variation tendency to the tested ratio, with the highest in  $0^\circ$  and  $90^\circ$ , lowest between  $30^\circ$  and  $60^\circ$ . Theoretically, the thicker the core is, the larger the Poisson's ratio of the sandwich in  $0^\circ$  and  $90^\circ$  will be, but lower between  $15^\circ$  and  $75^\circ$ . Thus, for sandwich structure with a thicker core, the theoretical correlation ratio by Eq. 12 is lower than that by Eq. 11 between  $15^\circ$  and  $75^\circ$ . But in  $0^\circ$  and  $90^\circ$ , the correlation ratio by Eq. 12 is almost the same as that by Eq. 11 even for the 60 mm thick core. And the max error between tested ratio and value by Eq. 12 is 18.58% in  $15^\circ$  for 60 mm cored sandwich. However, the error between average tested ratio and that obtained from Eq. 11 is only 14.30%. Hence, the influence of Poisson's ratio of the tested sandwich structures in Eq. 12 seems too accentuated to be applicable. In

addition, considering the acoustic wave propagation modes, due to the Poisson effect, the out-of-plane flexural wave has more influences on the received signals if the core is thicker, which will result in higher acoustic wave attenuation and measurement error. This phenomenon can also explain why the tested correlation ratio is much higher than the theoretical ratio by Eq. 11 and Eq. 12 for the thicker sandwich structure.

In conclusion, Eq. 11 can be effectively used to predict the AE wave velocity in most common sandwich structures from the velocity in the corresponding skin. Even though the core of the sandwich is thicker, the difference between average tested correlation ratio and calculation value by Eq. 11 should be acceptable. For core thickness smaller than 60 mm, the model proposed has been demonstrated to be accurate enough.

## 4.2. AE wave velocity in GFRP-balsa sandwich structure

### 4.2.1. Comparison of the measured velocity and calculated value

Substituting the specimen dimension and material parameters in Table 3 and Table 4 into Eq. 7, the density of the balsa cored sandwich specimen can be obtained:  $\rho_s(D) = 307 \text{ kg/m}^3$ .

In the similar way, AE wave velocity between  $0^\circ$  and  $90^\circ$  in the GFRP-balsa sandwich specimen can be calculated by Eq. 4 and then by Eq. 5 with the corrective factor equaling to 1.218.

The calculated velocities by the original model Eq. 4 (purple dotted line) and modified one Eq. 5 (blue dotted line) are compared to the measured values (red line), as shown in Fig. 12. The measured and analytical values show almost the similar variation tendency along different directions, with the highest velocity in  $90^\circ$  and the lowest in  $45^\circ$ . The max error of the results from the modified model Eq. 5 is reduced to 10.55% in  $15^\circ$ , compared to the max error 19.48% in  $90^\circ$  of the results from Eq. 4. The error is less reduced compared to that of the honeycomb sandwich structure, which is mainly due to the special anisotropic material property, higher acoustic attenuation and the adhesions of different balsa wood blocks in the balsa cored sandwich (see Fig. 2. (b)).

### 4.2.2. Correlation between AE wave velocity in the skin and sandwich

Fig. 13 compares the measured velocities in GFRP-balsa sandwich with those measured on the pure GFRP skin and balsa core. It is observed that AE wave velocity in the sandwich is always higher than that in the core but lower than that in the skin whatever the wave propagation direction is; the variation as a function of wave propagation directions in the sandwich and the skin have nearly the similar tendency, with the highest velocity in  $0^\circ$  and lowest in  $45^\circ$ .

Particularly, for pure balsa panel, the acoustic wave velocity is much lower, with lowest in  $0^\circ$  and within a range of 850-1000 m/s. It is interesting that the propagation direction has little effect on the acoustic wave velocity in balsa wood panel, with a very small standard deviation in each direction. This is mainly because the balsa panel is homogenized after the reconstruction of gluing small wood blocks, and it is a little different from the original anisotropic wood material. Compared to pure honeycomb core, balsa wood panel is less affected by the original material property.

For GFRP-balsa sandwich, the  $h_{c-\max}$  at  $\theta = 0^\circ$  for Eq. 11 is about 11 mm, so the model is acceptable for balsa core of 10 mm in this paper. Fig. 14 also shows that Eq. 12 gives the similar variation tendency to the tested values, with the highest in  $0^\circ$  and  $90^\circ$ , and lowest between  $30^\circ$  and  $60^\circ$ . The theoretical correlation ratio by Eq. 12 is almost the same as that by Eq. 11 in  $0^\circ$  and  $90^\circ$ , but much lower between  $15^\circ$  and  $75^\circ$ . Eq. 11 gives the value of the correlation ratio  $R = 0.75$ , which is consistent with the average measured ratio of 0.74. It demonstrates once again that Eq. 11 can be used to evaluate the AE wave velocity in any direction in the common sandwich structure from the velocity in the corresponding skin when  $h_c < 0.1h_f E_f(\theta)/E_c(\theta)$ , whatever the constituent materials are.

## 5. Conclusions

In this paper, Hsu-Nielsen AE tests are carried out to characterize the acoustic wave propagation velocity in the anisotropic composite laminate and sandwich structures. Velocity is proved to be an essential parameter for the damage localization by AE. The relationship between the AE wave velocity and the elastic modulus of the composite structure is investigated quantitatively by comparing the test results and the velocities calculated by an analytical model. These results are encouraging and they can benefit the future development of experimental and numerical models allowing to improve the damage localization of both the laminate and sandwich structures. The main conclusions include:

1. The traditional acoustic wave velocity formula has been extended to determine the AE wave propagation velocity in any direction in a composite laminate. And then the model is modified by introducing a corrective factor, which is defined as the ratio of the measured velocity over the calculated value in the  $0^\circ$  direction. Thus, only by measuring the wave velocity in  $0^\circ$ , the velocity in any direction of the composite structure can be predicted accurately and quickly, which can save a lot of experimental costs. Indeed, the calculated and

measured velocities show the similar variation tendency along different directions in the same composite laminate. It also indicates that the effects of propagation direction on the AE wave velocity cannot be ignored when localizing the damages by AE technique.

2. The modified acoustic wave velocity formula can also be effective for the complex composite sandwich structures, and results are similar to those of the thin laminate skins.
3. Due to the similar variation tendency of the AE wave velocity along different directions in the pure laminate skin and sandwich structure, it is possible to use the modified acoustic wave velocity formula to identify the velocity in the two types of structures from a calibration in one direction. A correlation ratio which reflects the direct relationship between the AE velocity in the sandwich and that in the skin is proposed. It is confirmed that AE wave velocity in the sandwich is dominated by the skin property, namely the elastic modulus of the skin, the density of the constituent materials, the core and skin thickness. As a consequence, the AE wave velocity in any direction in the sandwich structure can be predicted correctly by the velocity in the same direction in the skin panel when  $h_c < 0.1h_f E_f(\theta)/E_c(\theta)$ , whatever the constituent materials are.

In summary, based on this study, the AE wave velocity in a sandwich structure can be obtained either by the modified acoustic wave velocity formula or by the correlation ratio from the velocity in the corresponding skins. By the latter approach, velocity can be predicted without the complex fabrication process of the sandwich structure.

Eventually, a new 3-step strategy of rapid determination of AE wave propagation velocity is proposed for most usually used composite sandwich structures: 1- Measure the AE wave velocity of the composite skin in one direction; 2- Calculate the corrective factor proposed in this paper to determine the velocity in all directions of the composite skin by Eq. 5; 3- Determine the correlation ratio by Eq. 11, and then the velocity in any direction of a sandwich can be predicted.

Although the proposed method can predict rapidly the AE wave propagation velocity in any direction in a composite laminate or composite sandwich structure with acceptable precision, it is demonstrated that the relative error of the prediction could increase with the thickness of the sandwich core. In order to give quantitatively the relationship between the precision of the prediction and the core thickness, much more experimental and analytical works have to be realized in the future.

## Acknowledgements

The author Yuan Wu is supported by the China Scholarship Council for 3 years study at the University of Toulouse.

## Data availability

The raw data required to reproduce these findings are available to download from [INSERT PERMANENT WEB LINK(s)]. The processed data required to reproduce these findings are available to download from [INSERT PERMANENT WEB LINK(s)].

## References

- [1] Birman V, Kardomateas G A. Review of current trends in research and applications of sandwich structures. *Composites Part B: Engineering* 2018; 142: 221-240.
- [2] Amraei M, Shahravi M, Noori Z, et al. Application of aluminum honeycomb sandwich panel as an energy absorber of high-speed train nose. *Journal of Composite Materials* 2014; 48(9):1027-1037.
- [3] Mrazova M. Advanced composite materials of the future in aerospace industry. *Incas bulletin* 2013; 5(3): 139-150.
- [4] Arbaoui J, Schmitt Y, Pierrot J L, et al. Effect of core thickness and intermediate layers on mechanical properties of polypropylene honeycomb multi-layer sandwich structures. *Archives of Metallurgy and Materials* 2014; 59(1): 11-16.
- [5] Karakoç A, Freund J. Experimental studies on mechanical properties of cellular structures using Nomex® honeycomb cores. *Composite Structures* 2012; 94(6): 2017-2024.
- [6] Da Silva A, Kyriakides S. Compressive response and failure of balsa wood. *International Journal of Solids and Structures* 2007; 44(25): 8685-8717.
- [7] Borrega M, Gibson L J. Mechanics of balsa (Ochroma pyramidale) wood. *Mechanics of Materials* 2015; 84: 75-90.
- [8] Osei-Antwi M, De Castro J, Vassilopoulos A P, et al. Shear mechanical characterization of balsa wood as core material of composite sandwich panels. *Construction and Building Materials* 2013; 41: 231-238.
- [9] Zenkert D. An introduction to sandwich construction. *Engineering materials advisory services*, 1995.
- [10] Daniel I M, Gdoutos E E, Wang K A, et al. Failure modes of composite sandwich beams. *International journal of damage mechanics* 2002; 11(4): 309-334.
- [11] Ghobadi A. Common type of damages in composites and their inspections. *World Journal of Mechanics* 2017; 7(2): 24-33.
- [12] Garnier C, Pastor M L, Eyma F, et al. The detection of aeronautical defects in situ on composite structures using Non-Destructive Testing. *Composite Structures* 2011; 93(5): 1328-1336.
- [13] Dwivedi S K, Vishwakarma M, Soni A. Advances and Researches on Non-Destructive Testing: A Review. *Materials Today: Proceedings* 2018; 5(2): 3690-3698.

- [14] Dahmene F, Yaacoubi S, Mountassir M E L. Acoustic emission of composites structures: story, success, and challenges. *Physics Procedia* 2015; 70: 599-603.
- [15] Ammar I B, Karra C, El Mahi A, et al. Mechanical behavior and acoustic emission technique for detecting damage in sandwich structures. *Applied Acoustics* 2014; 86: 106-117.
- [16] Masmoudi S, El Mahi A, Turki S. Use of piezoelectric as acoustic emission sensor for in situ monitoring of composite structures. *Composites Part B: Engineering* 2015; 80: 307-320.
- [17] Sikdar S, Ostachowicz W, Pal J. Damage-induced acoustic emission source identification in an advanced sandwich composite structure. *Composite Structures* 2018; 202: 860-866.
- [18] Michalcová L, Bělský P, Petrusová L. Composite panel structural health monitoring and failure analysis under compression using acoustic emission. *Journal of Civil Structural Health Monitoring* 2018; 8(4): 607-615.
- [19] Baid H, Schaal C, Samajder H, et al. Dispersion of Lamb waves in a honeycomb composite sandwich panel. *Ultrasonics*, 2015; 56: 409-416.
- [20] Scarponi C, Briotti G. Ultrasonic technique for the evaluation of delaminations on CFRP, GFRP, KFRP composite materials. *Composites Part B: Engineering* 2000; 31(3): 237-243.
- [21] Noiret D, Roget J. Calculation of wave propagation in composite materials using the Lamb wave concept. *Journal of composite materials* 1989; 23(2): 195-206.
- [22] Morscher G N, Gyekenyesi A L. The velocity and attenuation of acoustic emission waves in SiC/SiC composites loaded in tension. *Composites science and technology* 2002; 62(9): 1171-1180.
- [23] Gorman M R. Plate wave acoustic emission. *The Journal of the Acoustical Society of America* 1991; 90(1): 358-364.
- [24] Prosser W H. Applications of advanced waveform-based ae techniques for testing composite materials. *Proceedings of the SPIE Conference on Nondestructive Evaluation Techniques for Aging Infrastructure and Manufacturing: Materials and Composites*, Scottsdale, Arizona, 2-5 December 1996.
- [25] Khon H, Bashkov O V, Zolotareva S V, et al. Modeling the Propagation of Elastic Ultrasonic Waves in Isotropic and Anisotropic Materials When Excited by Various Sources. *Materials Science Forum*. Trans Tech Publications 2019; 945: 926-931.
- [26] Gorman M R, Prosser W H. AE source orientation by plate wave analysis. *Journal of Acoustic Emission* 1991; 9(4): 283-288.
- [27] Yi Y, He J. Localizing acoustic emission sources in composite plates with unknown wave velocities. *7th Asia-Pacific Workshop on Structural Health Monitoring*, Hong Kong SAR, P.R. China, 12-15 November 2018.
- [28] Meo M, Zumpano G, Piggott M, et al. Impact identification on a sandwich plate from wave propagation responses. *Composite structures* 2005; 71(3-4): 302-306.
- [29] Albadr A, McCrory J, Holford K, et al. Effects of honeycomb core on acoustic emission wave propagation in glass fibre composite plates. *58th Annual British Conference on Non-Destructive Testing*, Telford, UK, 3-5 September 2019.
- [30] Benmadakhene S, Laksimi A. Propagation Study of Acoustic Emission Waves in Composite Materials. *Proceedings of the 13th ICCM*, Beijing, China, 25-29 Jun 2001.
- [31] Baydoun S K, Voigt M, Jelich C, et al. A greedy reduced basis scheme for multifrequency solution of structural acoustic systems. *International Journal for Numerical Methods in Engineering* 2020; 121(2): 187-200.
- [32] Dahle G A, James K R, Kane B, et al. A review of factors that affect the static load-bearing capacity of urban trees. *Arboriculture and Urban Forestry* 2017; 43(3): 89-106.
- [33] Malek S, Gibson L J. Multi-scale modelling of elastic properties of balsa. *International Journal of Solids and Structures* 2017; 113: 118-131.
- [34] Perrin M, Yahyaoui I, Gong X. Acoustic monitoring of timber structures: Influence of wood species under bending loading. *Construction and Building Materials* 2019; 208: 125-134.
- [35] Kee Paik J, Thayamballi A K, Sung Kim G. The strength characteristics of aluminum honeycomb sandwich panels. *Thin-Walled Structures* 1999; 35(3): 205-231.

**Figures (Color should be used for any figures in print.)**

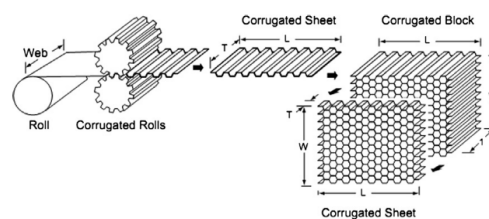
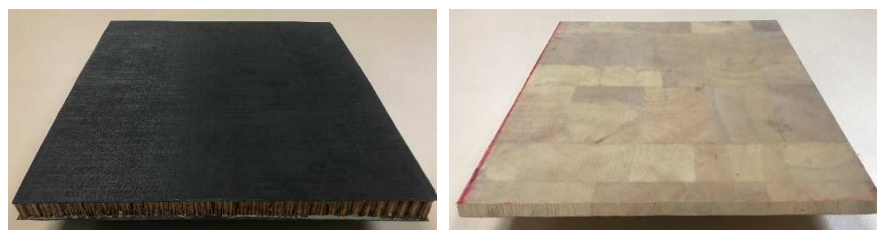


**Fig. 1.** L and W orientations of honeycomb core due to the fabrication process [5].



(a) (b)

**Fig. 2.** The tested sandwich panels: (a) CFRP-honeycomb sandwich panel. (b) GFRP-balsa sandwich panel.

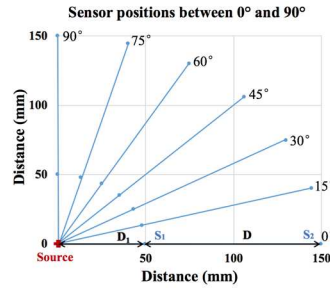


**Fig. 3.** Schematic diagram of the positions of sensors and source on the tested panel between 0° and 90°.

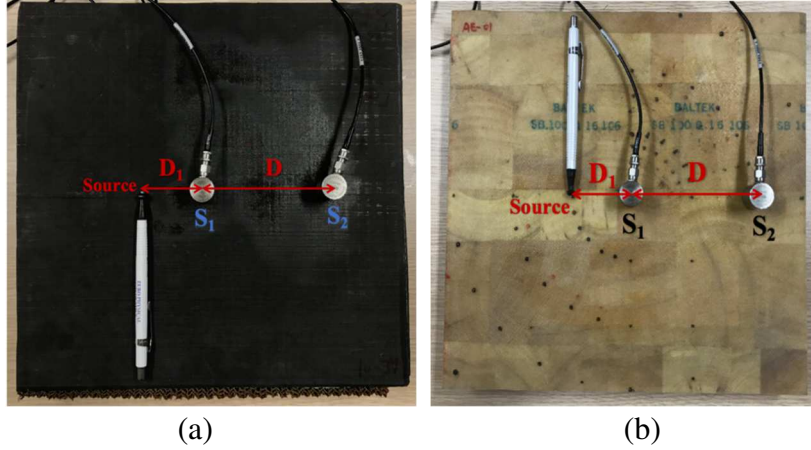


**Fig. 4.** Positions of the sensors and source (in 0° direction) on the tested sandwich panels: (a) CFRP-honeycomb sandwich panel. (b) GFRP-balsa sandwich panel.

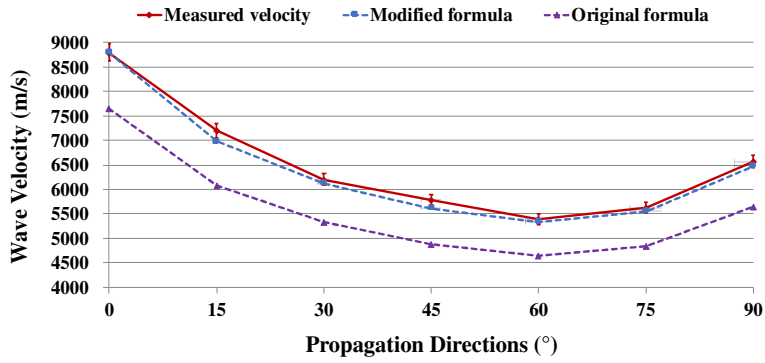


**Fig. 5.** Comparison of measured acoustic wave velocity and calculated value of [0°/90°/0°] CFRP panel.

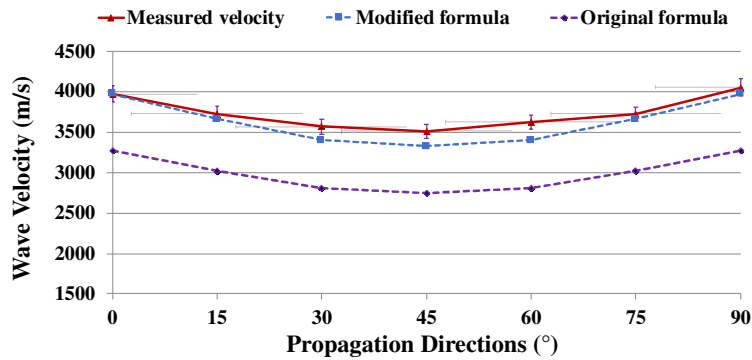


**Fig. 6.** Comparison of measured acoustic wave velocity and calculated value of 3-layer woven GFRP panel.

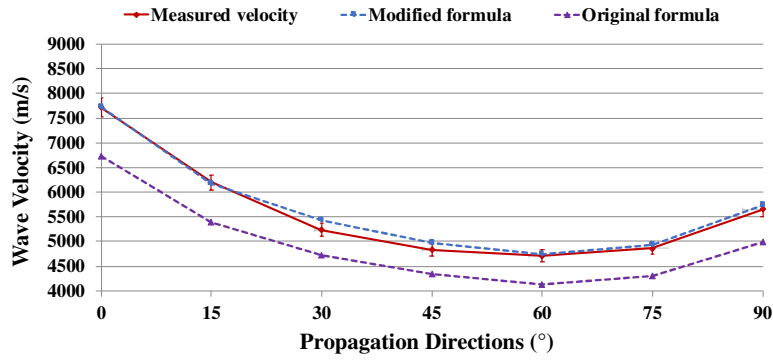


Fig. 7. Comparison of measured acoustic wave velocity and calculated value in CFRP-honeycomb sandwich A.

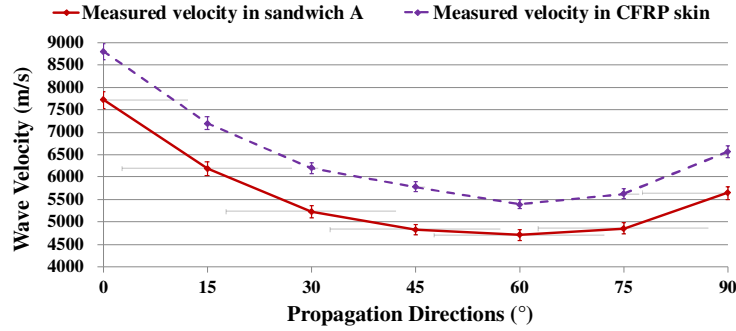


Fig. 8. Comparison of measured acoustic wave velocity in sandwich A and CFRP skin panel.

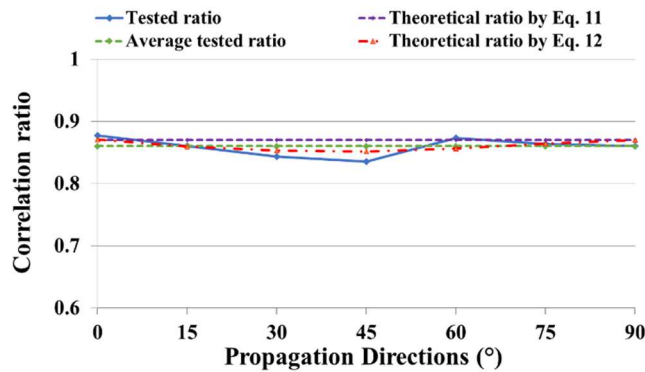


Fig. 9. Correlation ratio of AE wave velocity in CFRP-honeycomb sandwich A over that in the skin.

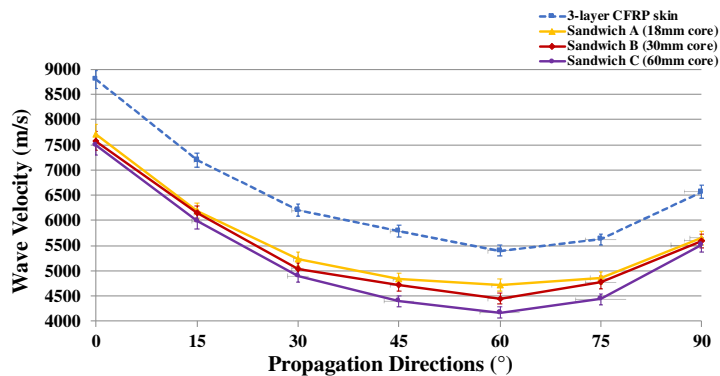
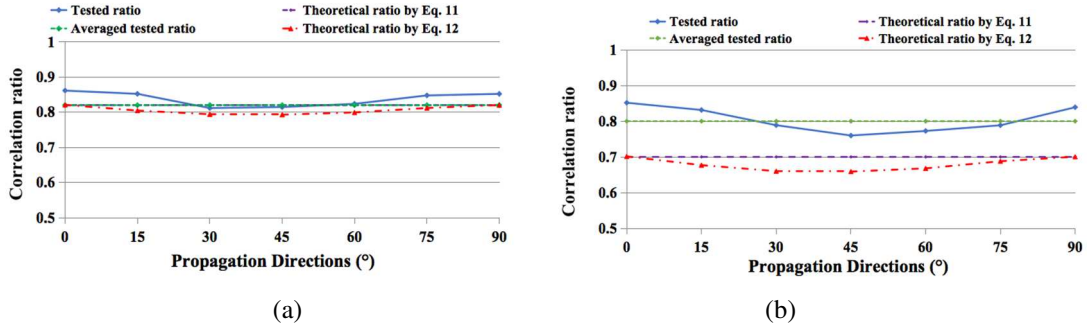
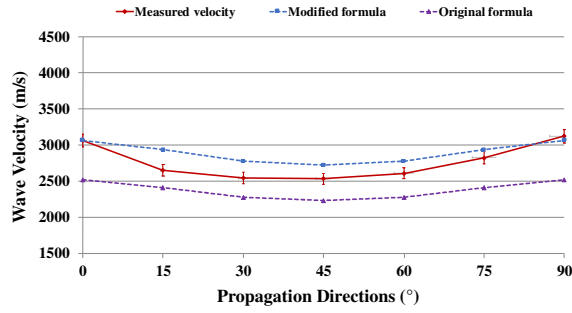


Fig. 10. Comparison of measured acoustic wave velocity in CFRP-honeycomb sandwich panels with different core thickness.



**Fig. 11.** Correlation ratio of AE wave velocity in CFRP-honeycomb sandwiches over that in the skins: (a) Correlation ratio of sandwich B. (b) Correlation ratio of sandwich C.



**Fig. 12.** Comparison of measured acoustic wave velocity and calculated values in GFRP-balsa sandwich.

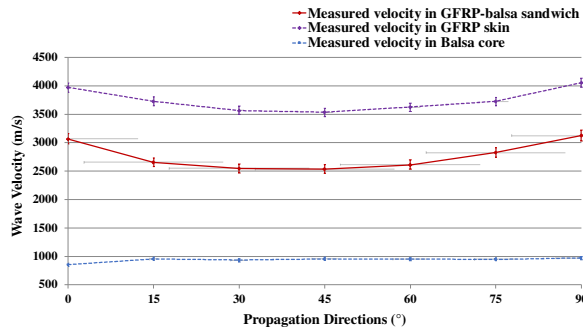


**Fig. 13.** Comparison of acoustic wave velocity in GFRP-balsa sandwich, GFRP skin and balsa core panel.

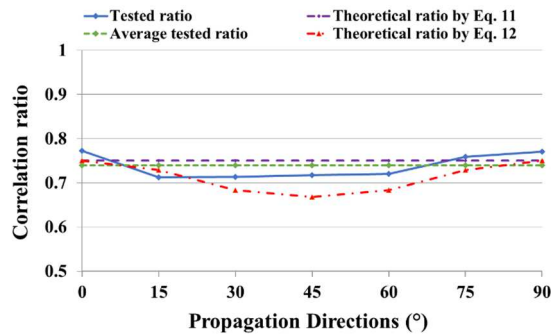


**Fig. 14.** Correlation ratio of AE wave velocity in GFRP-balsa sandwich over that in the skin.

**Tables**

**Table 1** CFRP-honeycomb sandwich specimen dimensions.

| Specimens | Core materials     | Length (mm) | Width (mm) | $h_s$ (mm) | $h_c$ (mm) | $h_f$ (mm) |
|-----------|--------------------|-------------|------------|------------|------------|------------|
| A         | Nomex honeycomb    | 300         | 300        | 19.5       | 18         | 0.75       |
| B         | Aluminum honeycomb | 300         | 300        | 31.5       | 30         | 0.75       |
| C         | Nomex honeycomb    | 300         | 300        | 61.5       | 60         | 0.75       |

Where  $h_s$ ,  $h_c$  and  $h_f$  are the thickness of the sandwich, the core and the skin, respectively.

**Table 2** Material parameters of CFRP-honeycomb sandwich.

| Constituents       | $E_1$ (GPa) | $E_2$ (GPa) | $G_{12}$ (GPa) | $\nu_{21}$ | $\rho$ (kg/m <sup>3</sup> ) |
|--------------------|-------------|-------------|----------------|------------|-----------------------------|
| Carbon fibr□T800H  | 152.4       | 9.2         | 4.3            | 0.35       | 1800                        |
| Nomex honeycomb    | 0.138       | 0.138       | 0.032          | 0.35       | 48                          |
| Aluminum honeycomb | 0.019       | 0.019       | 0.003          | 0.10       | 45                          |

**Table 3** GFRP-balsa sandwich specimen dimensions.

| Specimen | Core material | Length (mm) | Width (mm) | $h_s$ (mm) | $h_c$ (mm) | $h_f$ (mm) |
|----------|---------------|-------------|------------|------------|------------|------------|
| D        | Balsa wood    | 300         | 300        | 11         | 10         | 0.5        |

**Table 4** Material parameters of GFRP-balsa sandwich.

| Constituents                  | $E_1$ (GPa) | $E_2$ (GPa) | $G_{12}$ (GPa) | $\nu_{21}$ | $\rho$ (kg/m <sup>3</sup> ) |
|-------------------------------|-------------|-------------|----------------|------------|-----------------------------|
| Wov□n glass fibr□             | 20          | 20          | 2.85           | 0.13       | 1900                        |
| Balsa wood<br>(BALTEK SB.100) | 0.092       | 0.092       | 0.187          | 0.23       | 148                         |